Stress Shadows: Insights into Physical Models of Aftershock Triggering

Jeanne Hardebeck & Ruth Harris; US Geological Survey, Moffett Field, California, USA; jhardebeck@usgs.gov

USGS science for a changing world

Why do some aftershocks occur in stress shadows?

Hypothesis 1: Aftershocks appear to be in shadows because of inaccuracy in the stress change calculations.

Hypothesis 2: Aftershocks in the shadows occur on faults with different orientations than the model receiver faults, and these unexpected fault orientations experience increased Coulomb stress.

Hypothesis 3: Aftershocks in the shadows are triggered by another mechanism such as dynamic stress changes.

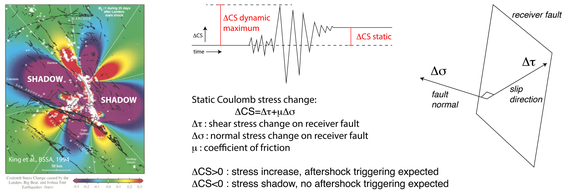

Hypothesis 1: Aftershocks appear to be in shadows because of inaccuracy in the stress change calculations (e.g. mainshock slip model, receiver fault orientation, friction).

Test 1: Many realizations of the stress calculations using multiple mainshock models, multiple receiver fault orientations based on the mechanisms of background events, and a range of coefficients of friction. Are any events persistently in the stress shadows?

Result 1: For 2016 Kumamoto, Japan, and 2019 Ridgecrest, California, sequences, hundreds of off-fault aftershocks have high probability (>70% of realizations) of being in stress shadows. ***Inconsistent with hypothesis.***

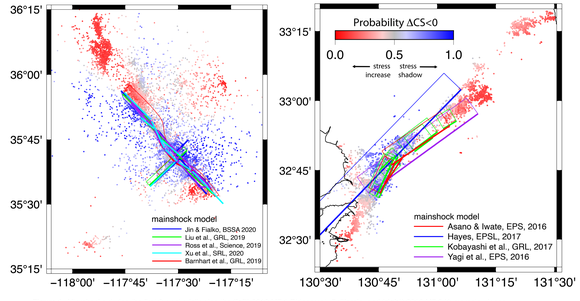

Figure 1. Aftershocks during the first 2 weeks following the **(left)** 2019 M7.1 Ridgecrest, California, and **(right)** 2016 M7.0 Kumamoto, Japan earthquakes. Events are color-coded by the probability that they occur in a stress shadow, defined as the fraction of realizations of stress change calculations that result in Coulomb stress change ΔCS<0. Mainshock source models are take from the SRCMOD Earthquake Source Model Database and literature, M~6 foreshocks included if source models are available, source models indicated by color. Mainshocks modeled as dislocations in an elastic half-space (Okada, BSSA 1992). Focal mechanisms of pre-mainshock earthquakes used as receiver faults for Coulomb stress calculation, multiple realizations sample their observed variation. Machine learning focal mechanism catalogs for Ridgecrest from Cheng et al. (JGR, 2023) and for Kumamoto from Uchide (GJI, 2020). Coefficient of friction μ sampled between 0.2 and 0.8.

Hypothesis 2: Aftershocks in the shadows occur on faults with different orientations than the model receiver faults, and these unexpected fault orientations experience increased Coulomb stress.

Test 2.1: Examine the variability of focal mechanisms of events in the shadows. Are they different from the background events?

Result 2.1: Mechanisms in the shadows are more diverse, and less consistent with background stress, than background events and aftershocks in stress increase regions. ***Consistent with hypothesis.***

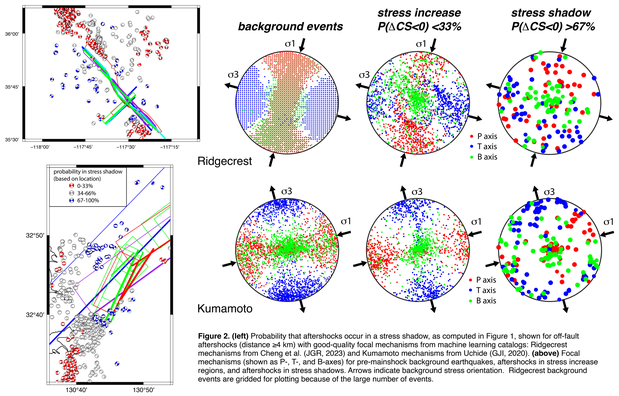

Figure 2. (left) Probability that aftershocks occur in a stress shadow, as computed in Figure 1, shown for off-fault aftershocks (distance ≥4 km) with good-quality focal mechanisms from machine learning catalogs: Ridgecrest mechanisms from Cheng et al. (JGR, 2023) and Kumamoto mechanisms from Uchide (GJI, 2020). **(above)** Focal mechanisms (shown as P-, T-, and B-axes) for pre-mainshock background earthquakes, aftershocks in stress increase regions, and aftershocks in stress shadows. Arrows indicate background stress orientation. Ridgecrest background events are gridded for plotting because of the large number of events.

Test 2.2: Are the individual event focal mechanisms consistent with an increase of Coulomb stress? Again, many realizations of the stress calculation, this time with individual event focal mechanisms as receivers.

Result 2.2: For both sequences, many of the events in the shadows also have low probability of a stress increase on the planes of their focal mechanisms. ***Inconsistent with hypothesis.***

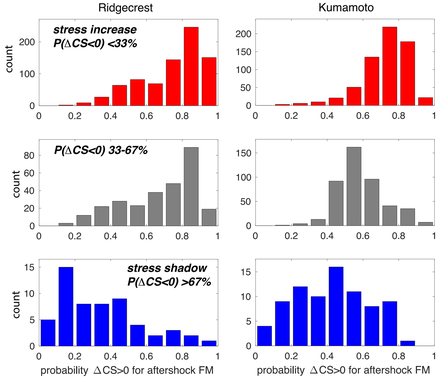

Figure 3. Probability than an earthquake experienced a positive Coulomb stress change, defined as the fraction of realizations of stress change calculations that result in Coulomb stress change ΔCS>0. Coulomb stress realizations as in Figure 2, except that the receiver faults are the fault planes of the focal mechanisms for the individual events, rather than the background mechanisms. The realizations sample the uncertainty of the focal mechanism, and coefficient of friction μ is sampled between 0.2 and 0.8.

Hypothesis 3: Aftershocks in the shadows are triggered by another mechanism such as dynamic stress changes.

Test 3.1: Are the spatial and temporal patterns of the aftershocks consistent with dynamic triggering?

Result 3.1: Aftershocks in shadows have spatial decay consistent with dynamic triggering by near-field body waves. They occur in an initial burst during first few days consistent with a transient process like dynamic triggering. (***Hardebeck & Harris, The Seismic Record, 2022***). ***Consistent with hypothesis.***

Spatial Decay

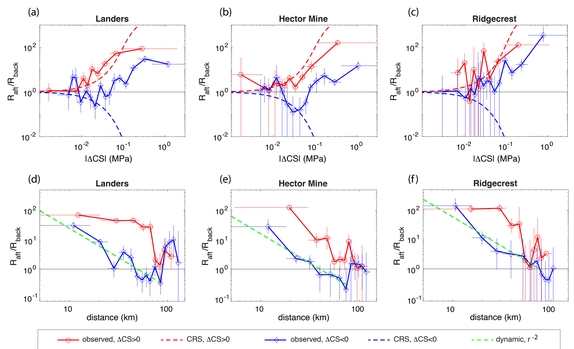

Figure 4. The spatial characteristics of aftershocks of three California sequences: 1992 M7.3 Landers, 1999 M7.2 Hector Mine, and 2019 M7.1 Ridgecrest. Aftershocks with positive (red circles) and negative (blue diamonds) static stress change areas plotted separately. **(a–c)** The ratio of the $M_{\geq}2$ aftershock rate over the first three months to background earthquake rate (Raft/Rback) as a function of the absolute value of the static Coulomb stress change |ΔCS|, along with static Coulomb Rate and State (CRS) model predictions (dashed curves) for positive and negative ΔCS at t=3 months. Horizontal error bars represent the range of values included in each stack, and the vertical error bars represent the uncertainty in Raft/Rback for the stack. **(d–f)** The ratio Raft/Rback as a function of distance from the closest point on the mainshock fault. A simple dynamic triggering model with $1/r^2$ is shown (dashed line). Mainshocks modeled as dislocations in an elastic half-space (Okada, BSSA 1992). Mainshock source models from Wald and Heaton (BSSA, 1994), Ji et al. (BSSA, 2002), and Liu et al. (GRL, 2019).

Temporal Decay

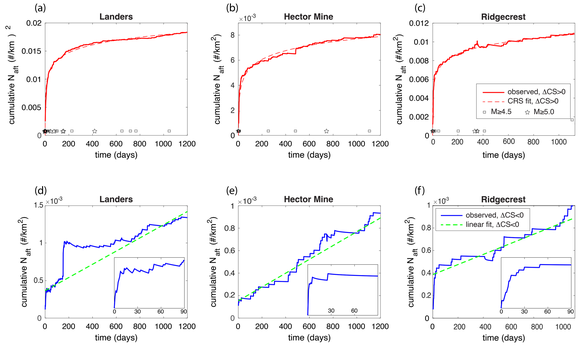

Figure 5. The temporal characteristics of aftershocks of three California sequences. The cumulative number of $M_{\geq}3$ aftershocks, Naft, is shown as a function of time after the mainshock, with the modeled number of secondary aftershocks removed using an ETAS model. **(a–c)** Cumulative number of aftershocks in positive stress change regions (red solid curve) and a Coulomb Rate and State (CRS) model fit to the observations (red dashed curve). Squares and stars show times of $M_{\geq}4.5$ and $M_{\geq}5$ aftershocks in the whole study area, respectively. **(d–f)** Cumulative number of aftershocks in stress shadows (blue solid curve) and a constant rate fit to the observations (green dashed line). Insets show the first 90 days, the time period shown in Figure 4. Note that the axis limits change between panels.

Hypothesis 3 continued: Aftershocks in the shadows are triggered by another mechanism such as dynamic stress changes.

Test 3.2: Are the aftershocks in the shadows consistent with triggering by the modeled dynamic stress changes?

Result 3.2: No evidence that aftershocks in shadows occur in locations or on fault planes with larger than typical dynamic stress changes, or with consistent patterns in the number of cycles, period, or duration of dynamic stresses.

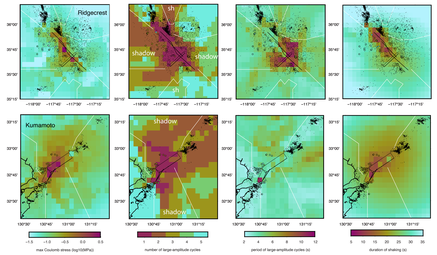

Figure 6. Stress metrics for dynamic stresses: maximum Coulomb stress change, number of cycles of large stress changes, period of large stress changes, and duration of dynamic stresses. Dynamic stresses modeled using the code of Cotton and Coutant (GJI, 1997) and the source models of Hirakawa & Barbour (BSSA, 2020) and Asano & Iwata (Earth Planets Space, 2016). Model periods ≥1 sec. Average value of metrics over multiple realizations with varying receiver fault orientation within its uncertainty. Coefficient of friction μ sampled between 0.2 and 0.8. Background grid shows dynamic stresses projected on background fault planes, filled circles show dynamic stresses projected on the fault planes of shadow aftershocks with A-C quality focal mechanisms (Cheng et al., JGR, 2023; Uchide, GJI, 2020). Black dots show other off-fault aftershocks (distance ≥4 km).

Shadow versus non-shadow aftershocks

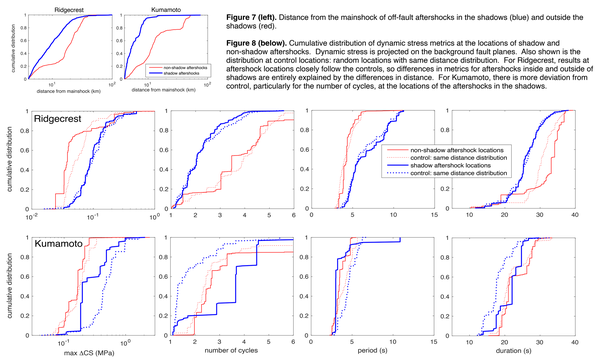

Figure 7 (left). Distance from the mainshock of off-fault aftershocks in the shadows (blue) and outside the shadows (red).

Figure 8 (below). Cumulative distribution of dynamic stress metrics at the locations of shadow and non-shadow aftershocks. Dynamic stress is projected on the background fault planes. Also shown is the distribution at control locations: random locations with same distance distribution. For Ridgecrest, results at aftershock locations closely follow the controls, so differences in metrics for aftershocks inside and outside of shadows are entirely explained by the differences in distance. For Kumamoto, there is more deviation from control, particularly for the number of cycles, at the locations of the aftershocks in the shadows.

Background fault planes versus aftershock focal mechanisms

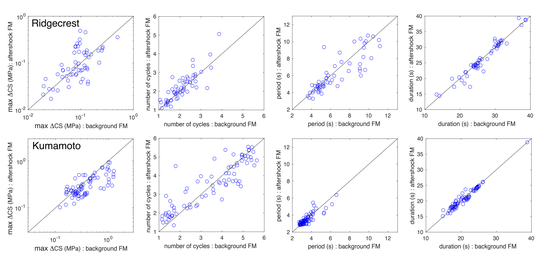

Figure 9. Dynamic stress metrics at the locations of shadow aftershocks, comparing dynamic stress projected on the aftershock focal mechanisms with dynamic stress projected on the background fault planes. Results scatter around the 1-to-1 line, except that Coulomb stress change at Kumamoto is slightly smaller on aftershock planes compared to background planes.